Proceedings of the ASME 2012 Summer Heat Transfer Conference
HT2012
July 8-12, 2012, Rio Grande, Puerto Rico

HT2012-58528

FLOW DESTABILIZATION AND HEAT TRANSFER AUGMENTATION IN AN ARRAY OF GROOVED PASSAGES WITH DEVELOPING FLOW

John Akerley
Graduate Research Assistant
Mechanical Engineering Department
University of Nevada, Reno
Reno, Nevada, USA

Miles Greiner
Professor of Mechanical Engineering
University of Nevada, Reno
Reno, Nevada, USA

Aleksandr Obabko
Assistant Computational Scientist
Argonne National Laboratory
Argonne, Illinois, USA

Paul Fischer
Senior Computational Scientist
Argonne National Laboratory
Argonne, Illinois, USA

ABSTRACT

In the current work, two-dimensional spectral element simulations are used to investigate the heat transfer and fan power performance of the developing regions of finite-length, grooved channel passage arrays, including the accelerating and decelerating flows entering and exiting the arrays. The performance of the grooved channel arrays is compared with that of flat passage arrays with the same average wall center-to-center spacing for Reynolds numbers ranging from 1000 to 3000. The simulations show that unsteadiness develops after a number of groove lengths and results in enhanced heat transfer. The unsteadiness improves the overall heat transfer compared with a flat passage array of equal average channel height by a factor of 1.46 at Re = 1000 and a factor of 2.75 at Re = 3000. The grooves also cause an increase in the required fan power by a factor of 8.56 at Re = 1000 and a factor of 18.10 at Re = 3000. Since past simulations have shown that three-dimensional simulations are necessary to accurately predict heat transfer and fan power performance in transversely grooved passages, the current two-dimensional results will be used as a starting point for a three-dimensional model that will ultimately be used to predict heat transfer and friction factor performance in developing grooved channel flows.

INTRODUCTION

Enhanced heat transfer surfaces are used frequently in a variety of practical devices, such as electronics, power plant condensers, and heating, ventilation and air conditioning devices [1]. Some of these enhancements use fins to extend surface areas or offset strips to promote thin boundary layers. In the past, researchers have considered passage configurations that enhance mixing and heat transfer by triggering flow instabilities. Transversely grooved channels [2-4], passages with eddy promoters [5,6], and communicating channels [7] all contain features whose sizes are roughly half the channel wall-to-wall spacing. These features promote inflections in the passage velocity profile. Kelvin-Helmholtz instabilities of these inflected profiles project energy onto normally damped Tollmien-Schlichting waves, resulting in two-dimensional traveling waves at moderately low Reynolds numbers.

Representative papers by the current authors have presented studies on flow destabilization in rectangular cross-section channels with transverse grooves cut into the walls [3,8-14]. Visualizations in a range of passage geometries with fully developed flow show that the critical Reynolds number, Re_c, where two-dimensional waves first appear decreases as the spacing between grooves decreases. For a sawtooth-shaped wall with no spacing between grooves, two-dimensional waves first appear at $Re_c = 350$, followed by a transition to three-dimensional mixing at Reynolds numbers greater than 500 [9].

Numerical and experimental investigations using air in a fully developed flow show that both the Nusselt number and friction factor are greater than the corresponding values for a flat channel with the same minimum wall-to-wall spacing

[3,14]. Three-dimensional numerical simulations for Re$\leq$ 2000 give results that are in good agreement with experimental measurements [10,11]. However, two-dimensional simulations were inadequate for capturing the transport processes in these configurations for Reynolds numbers greater than Re = 570 [10].

In recent years, researchers have given attention to other groove shapes or surface additions that limit the pressure drop within the channel. Studies have shown that semispherical dimples impressed on the surface of parallel-plate passages produced significant heat transfer augmentation with relatively small pressure drop [15,16]. The addition of curved vanes to grooved passages has also shown a reduction in pressure drop for Reynolds numbers of less than 400 [17,18]. The current work, however, returns to the sawtooth-geometry corresponding to the slowest decaying Tollmien-Schlichting waves [9].

Previous analyses focused on heat transfer augmentation with fully developed flow. However, air passage lengths in some practical heat transfer devices are less than fifty times the wall center-to-center spacing in order to take advantage of the heat transfer coefficients associated with developing flow. These configurations indicate that developing flow is important in practical passages and that the flow experiences significant acceleration at the channel entrance (due to the wall thickness and shape) and deceleration at its exit. Furthermore, since these devices use arrays of parallel passages, the interaction of the entrance and exit regions of neighboring grooved passages must be examined, which to our knowledge has yet to be done.

The current work is a numerical investigation of heat and momentum transport in an array of finite-length continuously grooved passages with developing flow. For Reynolds numbers ranging from 1000 to 3000, the average Nusselt number and fan power required to move the air through the arrays are calculated and compared with arrays with flat passages of equal wall center-to-center spacing. Arguably, three-dimensional simulations predict the pressure gradient and heat transfer in grooved passages much more accurately than do two-dimensional calculations [10,12]. The current two-dimensional simulations, however, offer an opportunity to learn more about this flow, while using less computational resources, and will provide guidance for future three-dimensional simulations.

NOMENCLATURE

a Groove length, Figure 1
b Groove depth, Figure 1
c_p Fluid specific heat
D_H Hydraulic diameter, $2H_A$
H_A Average channel height, Figure 1
H_M Minimum channel height
k Fluid thermal conductivity
L Channel array length, 30 grooves
L_E Exit region length, Figure 1, 25 grooves
L_I Inlet region length, Figure 1, 2.5 grooves
M Channel depth normal to page
Nu_L Average Nusselt number at $x_G = 30$
Nu_x Average Nusselt number between inlet and location x
P Pressure
Pr Fluid molecular Prandtl number, 0.70
Re Reynolds number, $u_0(2H_m)/\upsilon$
Re_c Critical Reynolds number
T Temperature
T_0 Inlet temperature, Figure 1
T_w Wall temperature
u Axial velocity
u_0 Inlet axial velocity, Figure 1
V Volume
w Wall thickness, Figure 1
x_G Groove coordinate, x/a

Greek

α Thermal diffusivity
ρ Fluid density
υ Fluid kinematic viscosity
Φ_L Non-dimensional fan power at $x_G = 50$
Φ_x Non-dimensional fan power at location x

NUMERICAL METHOD

Computational Domain

In the current work, a two-dimensional spectral element model was developed using the Nek5000 solver and mesh generator. Nek5000 is a mature DNS/LES computational fluid dynamics solver developed at the Mathematics and Computer Science Division at Argonne National Laboratory [19].

Figure 1 shows the two-dimensional spectral element mesh used in the current work to study an array of grooved passages. A simulated flow of air with Prandtl number 0.7 enters the left side of the entrance region (length of region is L_I) with a uniform dimensionless axial speed of u_0 = 1 and dimensionless temperature of T_0 = 0. The flow then encounters a pair of grooved channels (one above the other) at location x = 0 with length L. The passage walls are marked on Figure 1 with bold black lines and are modeled by using no-slip conditions and a uniform dimensionless temperature of T_w = 1. The flow exits the channel array into an exit region of length L_E. Because of domain size, Figure 1 shows a break in the channel array and in the exit region. Periodic boundary conditions are applied to the top and bottom edges of the inlet and exit regions to model an infinite number of channels stacked above and below the computational domain (the zigzag shape of the region boundaries are used for convenience, but flat boundaries would be equivalent).

In Figure 1, the groove depth normal the flow direction is b, length in the flow direction is a, the wall thickness normal to the flow direction is w, the average wall center-to-center spacing is H_A, and the minimum wall-to-wall spacing within the grooved channel is H_M. Previous studies have shown that the ratio a/H_M = 2.4 is compatible with the most slowly decaying

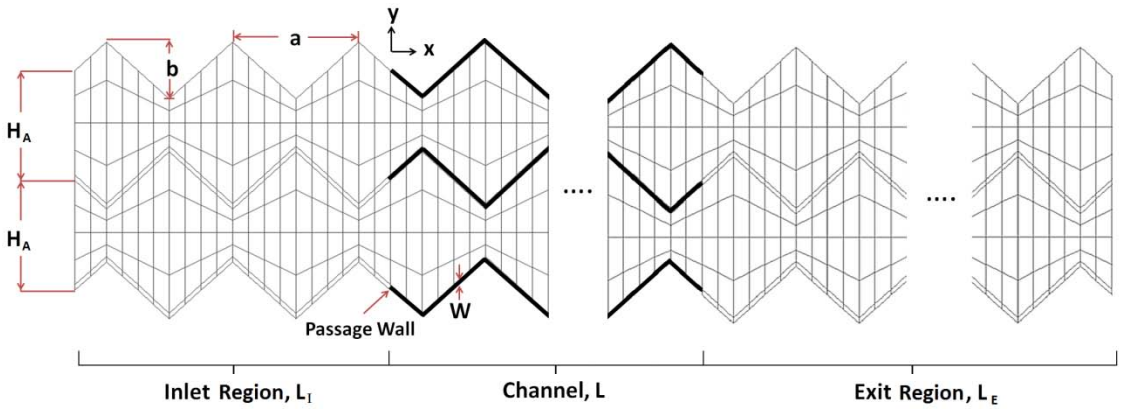

Figure 1 Computational domain and spectral element mesh.

Tollmien-Schlichting wave [4]. The dimensionless geometric parameters are a/b = 2, a/H_A = 0.925, b/H_A = 0.465, a/H_M = 2.4, w/H_A = 0.150, and H_M/H_A = 0.385. The length of the inlet region, channel, and exit region are, respectively, L_I = 2.5a, L = 30a, and L_E = 25a. Each groove length has 32 spectral elements.

Because of finite passage wall thickness, the cross section available for flow within the channels is smaller than that in the region. Figure 1 shows that the upper passage begins in a converging portion of a groove, while the lower one starts with a diverging section. The passages are an integer number of groove lengths long (30), so Figure 1 shows the upper passage ending in a converging section, while the lower ends with a diverging section.

The flow exits the domain using special outflow boundary conditions in the last vertical column of elements that avoids realization of reversed flow. The exit region is long to allow the unsteady flow exiting from the grooved channel to decay to a steady flow before it exits the domain. This allows the pressure recovery that takes place as the air decelerates (diffuses) outside the channel array to be calculated.

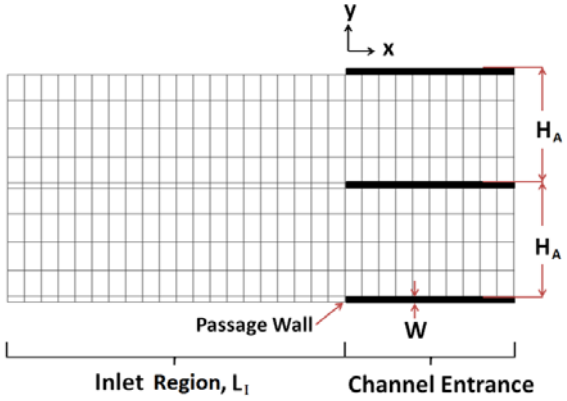

Figure 2 Spectral element mesh of inlet region and channel entrance for flat passage array.

Figure 2 shows the inlet region of a flat passage array used as a comparison with the grooved channel. The wall center-to-center spacing of these channels H_A is the same as the average wall center-to-center spacing of the grooved passage. The wall thickness in the direction normal to the flow direction, w, is also the same. As a result, the volume of the walls for the two configurations is also the same. The surface area of the grooved channel is $\sqrt{2}$ times larger than that of the flat passage.

The Spectral Element Method

In the spectral element method, the velocity, data, and geometry are expressed as tensor-product polynomials of degree N in each of K quadrilateral spectral element, corresponding to a total grid point count of roughly KN^2 [20]. Numerical convergence is achieved by increasing the spectral order N. The present calculations were carried out at a base resolution of K = 4120, N = 7 (Fig. 1 shows some spectral elements but not the KN^2 grid points). Resolution tests were performed for Re = 1000 and Re = 3000 at N = 7 and N = 11. The present simulations use consistent approximation spaces for velocity and pressure [21]. The momentum and pressure equations are advanced by first computing the convection term, followed by a linear Stokes Helmholtz and Poisson solve for the velocity and pressure terms, correspondingly. The characteristics-based operator-integration-factor splitting scheme used allows for Courant-Fredrichs-Lewy number as large as 2.5 while maintaining third-order accuracy in time. Full details of the method can be found in [20-24].

RESULTS

In this work, the hydraulic diameter is defined as follows.

$$D_H = \frac{4V}{A_p} = \frac{4LM(2H_A)}{4LM} = 2H_A$$

Here, V is the passage volume, A_P is the projected wetted area, and M is the length of the domain in the direction normal to the page. In previous studies, the hydraulic diameter was

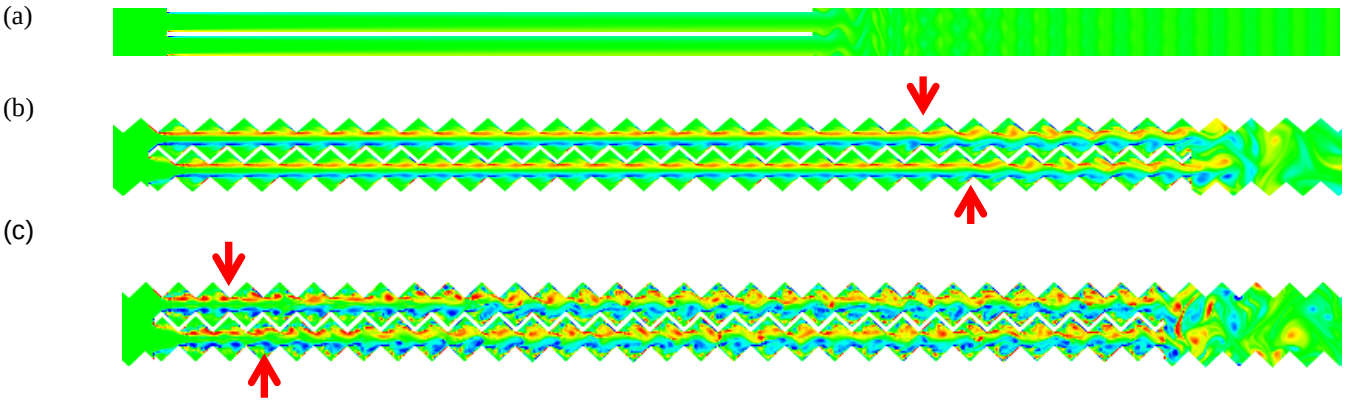

Figure 3 Fluid vorticity contour plots: (a) full domain flat passage at Re = 3000; (b) channel array at Re = 1000; (c) channel array at Re = 3000.

defined using the minimum wall-to-wall spacing. The use of the average wall center-to-center spacing offers a direct comparison to smooth passage arrays. The Reynolds number is defined as follows.

$$Re = \frac{u_0(2H_A)}{\upsilon} = \frac{2}{\upsilon}\int_B^T u\, dy$$

Here, υ is the fluid kinematic viscosity, and u is the axial component of the velocity. The integration is performed at a given x-location, from the bottom (B) to the top (T) of the domain. Since the flow rate is steady and the fluid is modeled to be incompressible, the integral is the same at all axial locations x and times t even though the flow is unsteady.

Figure 3 shows contour plots of fluid vorticity that are intended to help visualize the flow field. Figure 3a shows the entire computational domain for a flat passage array at Re = 3000. Figures 3b and 3c show a blowup focusing on the grooved channel arrays at Re = 1000 and 3000, respectively. Each contour is at an instant in time after the simulation has reached steady-state conditions.

In the flat passages, the vorticity contours are essentially parallel with the walls for all Reynolds numbers, indicating the flow is essentially parallel to the walls and is steady (the current two-dimensional simulations cannot model the three-dimensional instabilities that lead to turbulent flow in flat passages at Re > 2800 [25]).

Figure 3b shows that at Re = 1000, unsteadiness appears near the end of the grooved channels, roughly 24 groove lengths from the entrance ($x = 24a$) in the upper channel and 26 groove lengths from the entrance ($x = 26a$) in the lower channel. Figure 3c shows that at Re = 3000, unsteadiness appears near the channel entrance, roughly two groove lengths from the entrance in the upper channel and three groove lengths from the entrance in the lower channel. Arrows indicate these locations in Figures 3b and 3c. This onset location of oscillatory flow is different in each channel for four out of five Reynolds numbers investigated and moves upstream with an increasing Reynolds number.

The solid diamonds in Figure 4 show the observed onset location of oscillatory flow versus x/D_H from the current simulations based on the vorticity contour plots. Horizontal error bars indicate the difference in onset location between the upper and lower channels. These onset locations are highly qualitative and were determined based the observed change in fluid stream from steady to oscillatory. Only the simulation at Re = 2200 had the same axial onset location for the upper and lower channels. The onset location moves upstream with an increase in Reynolds number. For comparison, the onset location determined from experimental flow visualization data from a passage with one grooved and one flat wall is included from Greiner et al. 1990 [4]. The numerical results agree with experimental data at Re =1000. The experimental data also show that the onset location moves upstream with increasing Reynolds numbers. For Re > 1000 the experimental onset locations are further upstream than those from the current simulations. The level of unsteadiness entering the simulated channel is very low and may be higher in the experiments.

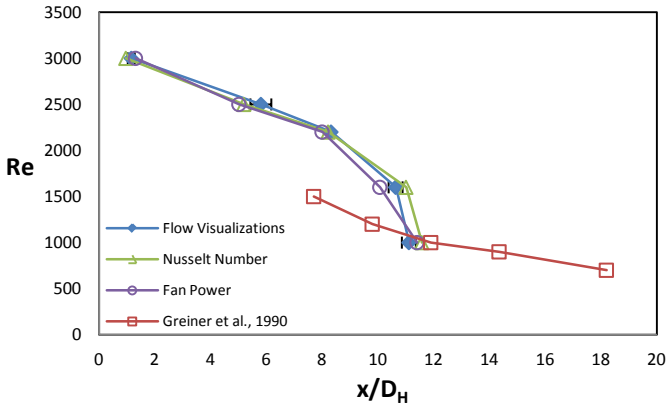

Figure 4 Observed onset location of oscillatory flow.

Future simulations may consider the effect of small levels of unsteadiness entering the channel to evaluate its effect on the onset location as well as three-dimensional effects.

In this work the average Nusselt number for a region between the inlet of the channel array and axial location x is defined as follows.

$$Nu_x = \frac{h_x x}{k} = \frac{\bar{Q}(x)}{A_{px}(T_w - T_0)}\frac{x}{k} = \frac{\rho c_p M \int_B^T (\overline{uT})_x \, dy}{4Mx(T_w - T_0)}\frac{x}{k}$$

$$= \frac{\int_B^T (\overline{uT})_x dy}{4\alpha}$$

The over bar $\bar{}$ denotes an average over time after the system has reached steady state, and the subscript $()_x$ indicates a value at the axial location x. In this definition, $\bar{Q}$(x) is the total heat transfer from all four walls to the fluid from between the entrance to location x, A_{px} = 4xM is the total *projected* surface area for both sides of the two walls from the entrance to x, and the temperature difference between the inlet gas and uniform temperature walls is $T_w - T_0 = 1 - 0 = 1$. The fluid specific heat, density, thermal conductivity and thermal diffusivity are, respectively, c_p, ρ, k and $\alpha = k/\rho c_p$.

Figures 5a and 5b show the average Nusselt number, Nu_x, versus groove coordinate, $x_G = x/a$, for Re = 1000 and Re = 3000, respectively. Each plot includes the grooved passage average Nusselt number for both lower (N=7) and higher (N=11) resolution grids and flat passage average Nusselt number (for N=7). Solid lines are used for the grooved channel heat transfer, while dashed lines are used for the flat passage results. For both Re = 1000 and 3000, the N = 7 and N = 11 results are nearly identical, indicating that the results are essentially grid independent.

Nu_x increases with x_G within the channel array because heat is transferred to the fluid in that region. It does not change upstream or downstream of the channels because there is no heat transfer outside of the channels.

For the flat passage arrays, the slope of the average Nusselt number decreases as the distance from the channel inlet increases. This rate of decrease is caused by the growth of the boundary layer. For the grooved passage arrays, the rate of decrease is less than that for the flat passages. Near the channel entrance, Nu_x is the same for both grooved and flat models but diverge after several groove lengths. This divergence location moves nearer the channel entrance with an increase in Reynolds number, similar to the behavior of the instability onset location. A slight change in curvature can be seen in the Nu_x versus x_G plots for grooved passages at Re = 1000 and 3000. The locations of these changes are indicated by arrows. The location of the change in curvature is plotted versus x/D_H in Figure 5 using open triangles. At each Reynolds number, this location is very close to the onset of unsteady flow locations described earlier (diamonds in Figure 4). This suggests that the slight curvature changes are caused by the onset of unsteady flow.

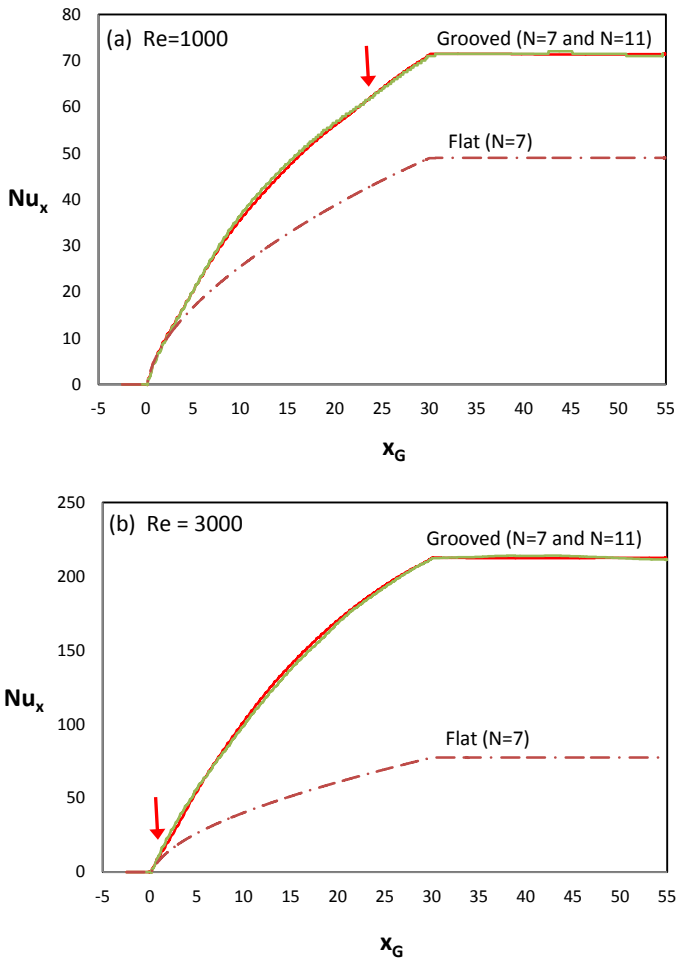

Figure 5 Average Nusselt number versus groove coordinate: (a) Re = 1000; (b) Re = 3000.

The full channel average Nusselt number, Nu_L, is the value of Nu_x at x_G = 30, and it characterizes the total heat transfer to the gas. Figure 6 shows the full channel average Nusselt number for both the grooved passages, $Nu_{L,G}$, and flat passages, $Nu_{L,F}$, versus Reynolds number. The heat transfer enhancement for a grooved array over a flat array increases with Reynolds number from a ratio of 1.46 at Re = 1000 to a ratio of 2.75 at Re = 3000. The dashed line marked $\sqrt{2}\,Nu_{L,F}$ shows the level of enhanced heat transfer that would be expected due to the area increase alone. It can be seen that most all of the enhancement is due to area increase at Re = 1000, and this is consistent with the onset of unsteady flow being near the channel exit at that Reynolds number (Figure 3b). Figure 6 shows that enhancement due to flow unsteadiness increases for Reynolds numbers greater than 1000. Figure 6

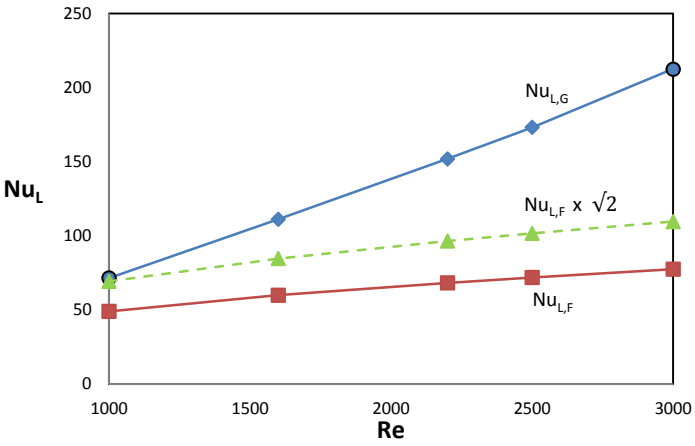

Figure 6 Average full channel Nusselt number versus Reynolds number.

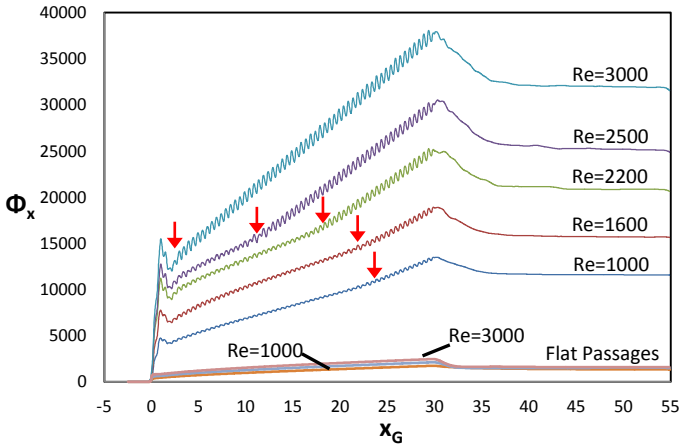

Figure 7 Non-dimensional fan power versus groove coordinate for Re = 1000, 1600, 2200, 2500 and 3000.

also includes the data from the N = 11 simulations at Re = 1000 and 3000. These are represented by open circles, and the values are nearly equal to the N = 7 results.

The dimensionless fan power or power required to move the gas against drag in the channel from its entrance at x = 0 to another x-location is defined as follows.

$$\Phi_x = \frac{1}{\rho u_0^2 v}\left[\int_B^T (\overline{uP})_{x=0}dy - \int_B^T (\overline{uP})_x dy\right]$$

Here, P is the pressure. Φ_x is similar to an area-average pressure drop between pressure at x = 0 and axial location x. Figure 7 shows the non-dimensional fan power versus x_G for Re = 1000, 1600, 2200, 2500 and 3000 for both grooved and flat passages. On the scale of this plot, the flat passage fan powers are very close to each other and only the upper (Re = 3000) and lower (Re = 1000) curves are marked. For all locations and Reynolds numbers the grooved passage flows require a significantly higher fan power than in the flat channel. For the grooved passage array at Re = 3000, the fan power exhibits a sharp increase at the channel entrance where the flow accelerates into the channel array. This acceleration is caused by blockage from the grooved wall's thickness and shape. The air must accelerate around this blockage as it enters the passage. Some of the pressure is recovered in the first few grooves as the velocity field becomes established. Further downstream, the fan power continues to increase due to drag within the channels. The fan power within the channel array oscillates as the flow accelerates and decelerates in the converging and diverging sections of the channel. The fan power decreases as the flow decelerates into the exit region where the pressure increases. The fan power and pressure reach their final values at roughly x_G = 45, which is 15 groove lengths downstream of the channel exit.

At lower Reynolds numbers, the fan power exhibits a similar behavior with a sharp increase at the channel entrance, small recovery, increase due to drag within the channel array, and decrease in the exit region. However, at lower Reynolds numbers the amplitude of the oscillations and the overall slope are small in a region near the inlet. Further downstream, the amplitude and slope both increase significantly. This location is marked by an arrow for each Reynolds number, and these locations are shown as Fan Power data points in Figure 4 (marked by open circles). These locations move upstream with an increase in Reynolds number and are in good agreement with the locations of the onset of flow unsteadiness and location where the Nusselt number exhibits a change in curvature. This suggests that the increase in amplitude and slope are caused by the onset of unsteady flow.

The flat passage fan power curves in Figure 7 exhibit a slight increase in the flat passage arrays at the channel entrance and a slight decrease at the channel exit. These changes are much smaller than those of the grooved channels because the flat passage blockage is much smaller. Fan power is significantly greater in the grooved passage arrays than in the flat passage arrays.

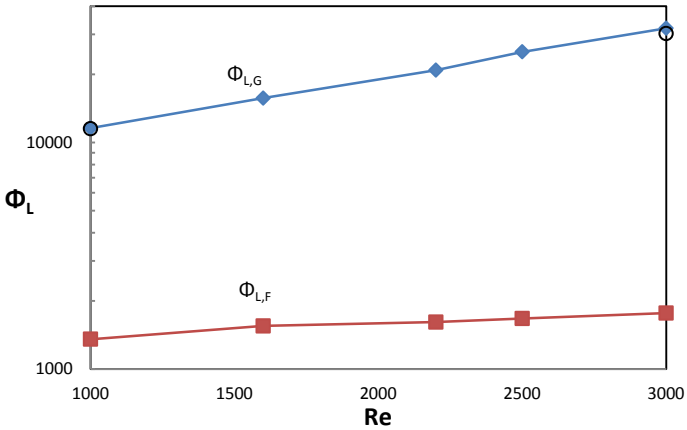

Figure 8 Non-dimensional fan power versus Reynolds number.

The full channel non-dimensional fan power, Φ_L, is the value of Φ_x at x_G = 50. It characterizes the total fan power required to accelerate the flow into the array, push the fluid through the array, and the recovery after it exits the array.

Figure 8 shows Φ_L versus Reynolds number for grooved ($\Phi_{L,G}$) and flat ($\Phi_{L,F}$) arrays. For all Reynolds numbers, the fan power is significantly greater in the grooved passage arrays than in the flat passage arrays. The required fan power also increases more significantly with Reynolds number in the grooved passage arrays than in the flat passage arrays. The fan power requirement for a grooved array over a flat array increases with Reynolds number from a ratio of 8.56 at Re = 1000 to a ratio of 18.10 at Re = 3000. Figure 8 also includes the data from the N=11 simulations at Re = 1000 and 3000, represented by open circles. The values are nearly equal to the N=7 results at Re = 1000, but slightly lower at Re = 3000.

Figure 9 shows Nu_L versus Φ_L for both grooved and flat passage arrays at Re = 1000, 1600, 2200, 2500 and 3000. Heat transfer augmentation can be achieved by using grooved passage arrays but only with a significant increase in the required fan power.

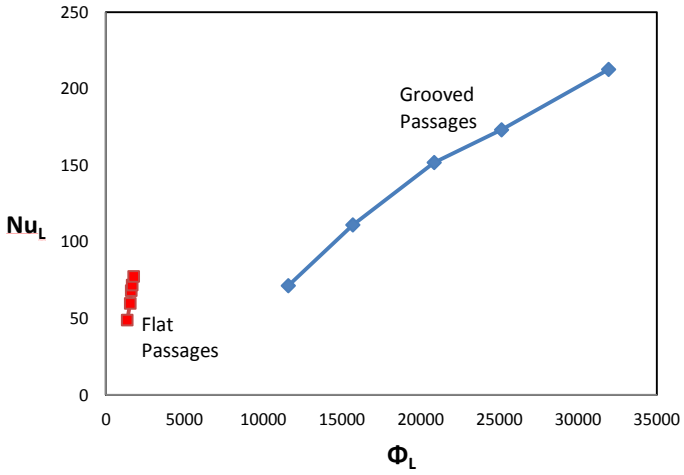

Figure 9 Full channel average Nusselt number versus non-dimensional fan power.

SUMMARY

Two-dimensional simulations of forced convection in an array of finite-length, continuously grooved passages with developing flow were performed by using the spectral element method for Reynolds numbers ranging from 1000 to 3000. The average Nusselt number and fan power were calculated in order to analyze performance of a grooved passage array compared with a flat passage array.

Steady-state results show that the addition of transverse grooves to the parallel passage arrays introduces unsteadiness a number of grooves downstream of the channel entrance. This onset location moves closer to the channel entrance as the Reynolds number increases. The unsteadiness improves the overall heat transfer compared with a flat passage array of equal average channel height by a factor of 1.46 at Re = 1000 and a factor of 2.75 at Re = 3000. The grooves also cause an increase in the required fan power by a factor of 8.56 at Re = 1000 and a factor of 18.10 at Re = 3000. However, these two-dimensional results may not adequately capture the entire instability and mixing structures that have been seen in experiments and three-dimensional simulations. These results will be used as an initial condition for future three-dimensional simulations.

FUTURE WORK

This paper did not explore the effects of neighboring passages on the pressure recovery in the exit region. A single grooved channel mesh with the same groove geometry will be used to compare the full channel fan power with the grooved channel array. The effects of an initial unsteadiness entering the grooved passage arrays as well as the effect of groove depth b on the onset location of unsteadiness will also be explored. A three-dimensional computational domain will be constructed to explore the structures that cannot be seen with two-dimensional simulations. An experimental apparatus is currently under construction to benchmark these results.

ACKNOWLEDGMENTS

This paper describes work performed by the University of Nevada, Reno for the U.S. Department of Energy under Contract DE-EE0003231. The work of J. Akerley was funded by the University of Nevada, Reno Fellowship in Material and Thermal Science for Nuclear Power under Contract NRC-38-10-949. The work of A. Obabko and P.F. Fischer was funded by the Mathematics and Computer Science Division of Argonne National Laboratory supported by the Office of Advanced Scientific Computing Research and Office of Science, U.S. Department of Energy, under Contract DE-AC02-06CH11357.

REFERENCES

[1] Webb, R.L., 2005, *Principles of Enhanced Heat Transfer*, second edition, Taylor & Francis, New York.

[2] Ghaddar, N.K., Korczak, K., Mikic, B.B., and Patera, A.T., 1986, "Numerical Investigation of Incompressible Flow in Grooved Channels. Part 1: Stability and Self-Sustained Oscillations," *J. Fluid Mech.*, Vol. 168, pp. 541-567

[3] Greiner, M., Chen, R.F., and Wirtz, R.A., 1991, "Enhanced Heat Transfer/Pressure Drop Measured from a Flat Surface in a Grooved Channel," *J. Heat Transfer*, Vol. 113, pp. 498-501.

[4] Roberts, E.P.L., 1994, "A Numerical and Experimental Study of Transition Processes in an Obstructed Channel Flow," *J. Fluid Mech.*, Vol. 260, pp. 185-209.

[5] Karniadakis, G.E., Mikic, B.B., and Patera, A.T., 1988, "Minimum-Dissipation Transport Enhancement by Flow Destabilization: Reynolds Analogy Revisited," *J. Fluid Mech.*, Vol. 192, pp. 365-391.

[6] Kozlu, H., Mikic, B.B., and Patera, A.T., 1988, "Minimum-Dissipation Heat Removal by Scale-Matched

Flow Destabilization," *Int. J. Heat Mass Transfer*, Vol. 31, pp. 2023-2032.
[7] Amon, C.H., Majumdar, D., Herman, C.V., Mayinger, F., Mikic, B.B. and Sekulic, D.P., 1992, "Experimental and Numerical Investigation of Oscillatory Flow and Thermal Phenomena in Communicating Channels," *International J. Heat Mass Transfer*, Vol. 35, pp. 3115-3129.
[8] Greiner, M., 1987, "Flow Field Destabilization and Heat Transfer in Grooved Channels," ASME FED-Vol. 52, pp. 131-138.
[9] Greiner, M., Chen, R.F. and Wirtz, R.A., 1990, "Heat Transfer Augmentation through Wall Shape Induced Flow Destabilization," *J. Heat Transfer*, Vol. 112, No. 2, pp. 336-341.
[10] Greiner, M., Spencer, G., and Fischer, P.F., 1998, "Direct Numerical Simulation of Three-Dimensional Flow and Augmented Heat Transfer in a Grooved Channel," *J. Heat Transfer*, Vol. 120, pp. 717-723.
[11] Greiner, M., Faulkner R.J., Fischer, P.F., and Wirtz, R.A., 1997, "Simulations of Three-Dimensional Flow and Augmented Heat Transfer in a Symmetrically Grooved Channel with Constant Temperature Walls," *J. Heat Transfer*, Vol. 122, pp. 653-660.
[12] Greiner, M., Fischer, P.F., Tufo, H.M., and Wirtz, R.A., 2002, "Three Dimensional Simulations of Enhanced Heat Transfer in a Flat Passage Downstream from a Grooved Channel," *J. Heat Transfer*, Vol. 124, pp. 169-176.
[13] Greiner, M., Fischer, P.F. and Tufo, H.M., 2002, "Two-Dimensional Simulations of Enhanced Heat Transfer in an Intermittently Grooved Channel," *J. Heat Transfer*, Vol. 124, pp. 538-545.
[14] Wirtz, R.A., Huang, F., and Greiner, M., 1999, "Correlation of Fully Developed Heat Transfer and Pressure Drop in a Symmetrically Grooved Channel," *J. Heat Transfer*, Vol. 121, pp. 236-239.
[15] Ridouane, E.H. and Campo, A., 2007, "Heat Transfer and Pressure Drop Characteristics of Laminar Air Flows Moving in a Parallel-Plat Channel with Transverse Hemi-Cylindrical Cavaties," *Int. J. Heat Mass Transfer*, Vol. 50, pp. 3913-3924.
[16] Ridouane, E.H. and Campo, A., 2008, "Heat Transfer Enhancement of Air Flowing Across Grooved Channels: Joint Effects of Channel Height and Groove Depth," *J. Heat Transfer*, Vol. 130, 021901.
[17] Herman, C. and Kang, E., 2002, "Heat Transfer Enhancement in a Grooved Channel with Curved Vanes," *Int. J. Heat Mass Transfer*, Vol. 45, pp. 3741-3757.
[18] McGarry, M., Campo, A. and Hitt, D.L., 2004, "Numerical Simulations of Heat and Fluid Flow in Grooved Channels with Curved Vanes," *Numer. Heat Transfer*, Part A, Vol. 46, pp. 41-54.
[19] Fischer, P.F., Lottes, J.W., and Kerkemeier, S.G., 2008 "Nek5000 Web Page," http://nek5000.mcs.anl.gov.
[20] Patera, A.T., 1984, "A Spectral Element Method for Fluid Dynamics; Laminar Flow in a Channel Expansion," *J. Comput. Phys.*, Vol. 54, pp. 468-488.
[21] Fischer, P.F., 1997, "An Overlapping Schwarz Method for Spectral Element Solution of the Incompressible Navier-Stokes Equations," *J. of Comput. Phys.*, Vol. 133, pp. 84-101.
[22] Fischer, P.F. and Patera, A.T., 1991, "Parallel Spectral Element Solutions of the Stokes Problem," *J. Comput. Phys.*, Vol. 92, pp. 380-421.
[23] Fischer, P.F. and Patera, A.T., 1992, "Parallel Spectral Element Solutions of Eddy-Promoter Channel Flow," *Proc. Of the European Research Community on Flow Turbulence and Computation Workshop*, Lausanne, Switzerland, Cambridge University Press, pp. 246-256.
[24] Fischer, P.F. and Ronquist, E.M., 1994, "Spectral Element Methods for Large Scale Parallel Navier-Stokes Calculations," *Comp. Meth. Mech. Engr.*, pp. 69-76.
[25] Fox, R.W., and McDonald, A.T., 1985, *Introduction to Fluid Mechanics*, third edition, John Wiley & Sons, New York, p. 338.